

Statistical Study of Low-Energy Heliosphere Particle Fluxes from 1.4 to 5 AU over a Solar Cycle

C. Denker¹, J. Z. Reza¹, A. J. Nelson¹, J. D. Patterson², T. P. Armstrong², C. G. MacLennan³, and L. J. Lanzerotti^{1,3}

Abstract. Throughout the entire Ulysses mission, the Heliosphere Instrument for Spectra, Composition, and Anisotropy at Low Energies (HI-SCALE) has collected measurements of low-energy interplanetary ions and electrons. Time-series of electron, proton, and ion fluxes have been obtained since 1990. We present statistical studies of high-resolution ion and electron energy spectra (~ 50 keV to ~ 5 MeV) as measured by the HI-SCALE instrument on the Ulysses spacecraft over a time interval longer than a solar cycle (1990 to 2004). Ulysses is the only spacecraft that continually measured the inner (~ 1.4 to ~ 5 AU) heliosphere particle population during these years. The data thus provide measures of the lower energy population of particles that a spacecraft traveling outward from Earth would have encountered, and that also could have impacted the atmosphere and surface of Mars and the surfaces of the Martian satellites, Phobos and Deimos, during this interval. Comparisons of Ulysses particle fluxes with those from the Electron, Proton, and Alpha Monitor (EPAM) instrument on the Advanced Composition Explorer (ACE) spacecraft (the HI-SCALE back-up instrument) have shown that it is common for the particle fluxes in the inner heliosphere following solar events to be distributed quite uniformly in heliolatitude. Thus, the Ulysses measurements, while taken over a range of heliolatitudes, can provide important statistical information that can be used to estimate the low-energy radiation dosages and potential sputtering fluxes to planetary surfaces and to heliosphere spacecraft surfaces and solar arrays over a solar cycle.

1. Introduction

The increased interest in exploration (by robotic and human systems) of solar system objects – the Moon and potentially Mars – has rekindled considerable attention on the practical implications to spacecraft systems and to humans of the charged particle radiation environment outside Earth’s magnetosphere and beyond 1 AU [e.g., Foullon *et al.*, 2005; Parker, 2005]. This paper addresses the statistics of the low-energy electron and proton radiation (~ 50 keV to ~ 5 MeV) beyond 1 AU as measured with the HI-SCALE instrument [Lanzerotti *et al.*, 1992] on the Ulysses spacecraft during the last decade and one-half – covering more than a solar cycle.

The only space probe that has provided continuous data coverage in the heliosphere between the orbits of Earth and Jupiter [e.g., Boufaïda and Armstrong, 1997] is the solar polar-orbiting Ulysses spacecraft, a joint collaborative mission by ESA and NASA. Launched in 1990, Ulysses has operated flawlessly to date, providing unique data on the interplanetary environment beyond Earth’s orbit. Studies of the statistical distributions over more than one solar cycle of the charged particle fluxes as returned from Ulysses can provide some measures of the radiation environment that a spacecraft might be expected to encounter between 1 and 5 AU. A similar statistical study, obtained with the Earth-orbiting Interplanetary Monitoring Platform 8, shows the solar cycle variations in energy spectra of solar and interplanetary particles over 27 years from 1973 to 2000 [Simunac and Armstrong, 2004].

The energies of the particles whose statistical distributions are presented in this paper are sufficiently low that they will be stopped

in any sensible spacecraft or spacesuit materials, and hence will in general be of little importance for considerations of human safety. However, such particle fluxes can be of potential importance for their impact on, and sputtering and modification of, spacecraft surface materials and solar arrays, and for their effects in altering the surfaces of naturally-occurring objects in this region of the heliosphere. Such naturally-occurring objects range from icy and solid dust grains [e.g., Lanzerotti *et al.*, 1978; Johnson, 1990] to the atmospheres and surfaces of the Moon, Mars, and its natural satellites Phobos and Deimos. Data on higher energy particles of more relevance to human safety were acquired by other instruments on Ulysses, and analyses of these data similar to those presented here would be of benefit to an exploration program.

While the Moon and Mars are confined to the ecliptic plane, Ulysses spends much of its orbit outside the ecliptic, passing as high as 80° heliolatitude over the north and south solar poles. Nevertheless, research in recent years using data from Ulysses and from the 1 AU in-ecliptic ACE spacecraft has demonstrated that solar activity (flares, filament eruptions, and coronal mass ejections (CMEs)) can fill the heliosphere with a “reservoir” of particles independent of heliolatitude. Such a reservoir slowly decays away with time, of order of many days or more [Roelof *et al.*, 1992; MacLennan *et al.*, 2003]. That is, solar activity, whether from near the solar equator or at mid-solar latitudes, can produce particle fluxes that are soon found to be distributed reasonably uniformly in intensity over heliolatitudes. This feature of the heliosphere is important for understanding the particle environment in the range from ~ 1 to 5 AU. The latitude dependence at solar minimum of particles in the inner heliosphere has been presented by Patterson and Armstrong [2003].

During solar minimum, except near apogee in its orbit, Ulysses will neither measure particles in the near-ecliptic current sheet nor the effects of the current sheet in accelerating particles (including at co-rotating interactions regions, CIRs). Above the heliosphere current sheet, the fluxes of particles are measured to be very low [e.g., Lanzerotti *et al.*, 1995; Simpson *et al.*, 1995]. However, this solar minimum limitation in the statistics to be discussed in the subsequent sections is not a serious limitation of this study in that the

¹New Jersey Institute of Technology, Center for Solar-Terrestrial Research, 323 Martin Luther King Blvd, Newark, NJ 07102, USA

²Fundamental Technologies, 2411 Ponderosa, Suite A, Lawrence, KS 66046, USA

³Bell Laboratories, Lucent Technologies, 600 Mountain Avenue, Murray Hill, NJ 07974, USA

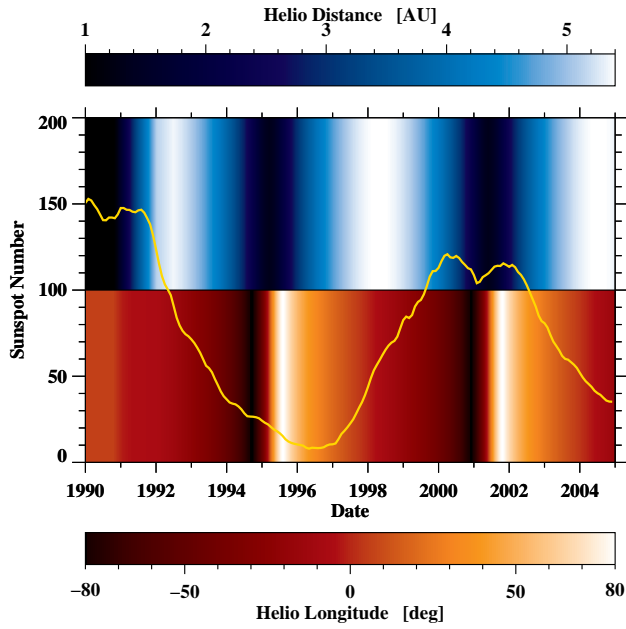


Figure 1. Smoothed monthly sunspot number (yellow curve) and position of the Ulysses spacecraft.

solar maximum fluxes (which become the particle reservoirs) are of sufficient intensity to be the dominant player when determining the longer-term implications of the heliosphere radiation environment beyond earth orbit.

2. Heliosphere Instrument for Spectra, Composition, Anisotropy and Low Energies

The HI-SCALE instrument was designed and built by the Applied Physics Laboratory (APL) of the Johns Hopkins University (JHU) to make measurements of low-energy ions and electrons [Lanzerotti *et al.*, 1992]. The instrument consists of five separate solid state detectors which uniquely identify ions with energies greater than 50 keV and electrons with energies greater than 30 keV. These five telescopes are divided into three distinct sys-

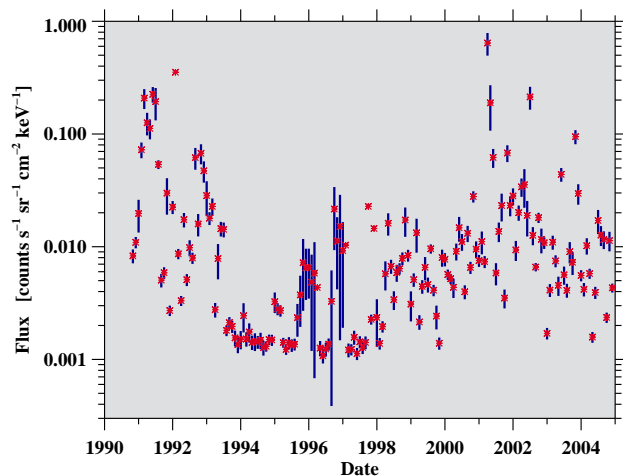


Figure 2. Monthly averages of the LEFS 150 proton flux in the 531 keV energy channel from 1990 to 2004.

Table 1. Power Law Fits to Proton and Electron Energy Spectra shown in Figures 4 and 5.^a

Year	Protons		Electrons	
	k	χ^2	k	χ^2
1990	-1.77	0.0124	-2.46	0.069
1991	-1.42	0.0019	-1.77	0.015
1992	-2.14	0.0838	-1.42	0.026
1993	-1.61	0.0303	-2.20	0.426
1994	-1.41	0.2232	-2.24	0.289
1995	-1.32	0.2181	-1.10	0.547
1996	-1.50	0.3196	-1.27	1.167
1997	-1.46	0.5673	-1.93	0.340
1998	-1.52	0.0299	-1.95	0.082
1999	-1.87	0.0588	-1.79	0.081
2000	-1.46	0.0054	-1.91	0.041
2001	-1.40	0.0048	-1.88	0.046
2002	-1.50	0.0053	-2.12	0.051
2003	-1.42	0.0085	-2.15	0.106
2004	-1.63	0.0291	-1.97	0.132
Average	-1.56	0.1056	-1.88	0.228

^a Power law model: $\Phi \sim E^k$, where Φ indicates the particle flux, E refers to the particle energy, and k is the exponent of the fit. The parameter χ^2 represents the unreduced goodness-of-fit statistic. The χ^2 -statistics indicate in all cases that the model parameters of the power law fit are “believable”.

tems: the Low-Energy Magnetic/Foil Spectrometers (LEMS30 & 120/LEFS60 & 150) and the Composition Aperture (CA).

High-resolution ion and electron energy spectra are obtained in a dedicated observing mode with lower temporal resolution (~ 17 -minute cadence) than the normal data collection mode with much better temporal resolution (~ 1 s cadence). In this high-energy resolution mode, the electrons are measured in 12 different energy channels ranging from 44 keV to 324 keV and protons/ions in 24 channels ranging from 66 keV to 4.10 MeV. The particle data collected by the LEFS60 and LEMS120 telescopes are acquired in eight unique, direction-of-arrival sectors, while the LEFS150 and LEMS30 telescopes involve four sectors.

The data have been carefully calibrated and formatted such that they are easily accessible for a broad user community [Patterson, 2002]. Currently, data reside in data servers at JHU APL (<http://sd-www.jhuapl.edu/Ulysses/>), the Coordinated Data Analysis Web (CDAWeb, <http://cdaweb.gsfc.nasa.gov/>), the National Space Science Data Center (NSSDC, <http://nssdc.gsfc.nasa.gov/>), and Fundamental Technologies (FunTec, <http://hiscale.ftcc.com/>). The input data for the statistical studies presented here are formatted as ASCII text and cover the interval from November 14, 1990 to De-

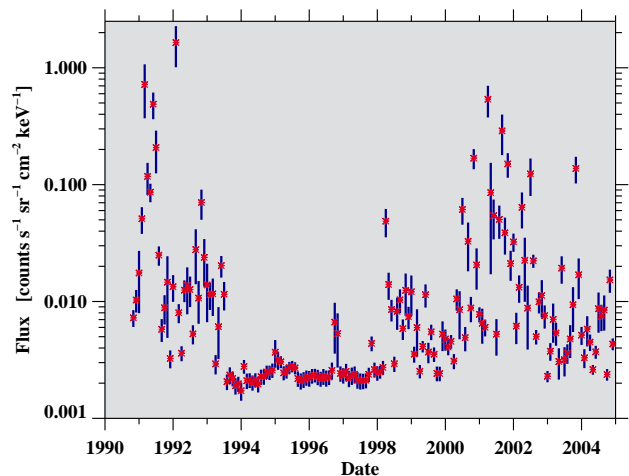


Figure 3. Monthly averages of the LEFS 150 electron flux in the 268 keV energy channel from 1990 to 2004.

cember 31, 2004 covering 14 years (5162 days) including two solar maxima (1991 and 2001) and one minimum (1995).

The smoothed monthly sunspot numbers (<http://www.ngdc.noaa.gov/stp/SOLAR/>) are shown in Figure 1 as a yellow curve, which is superposed on the background image depicting the position of Ulysses (heliolatitude and distance from the Sun). Figure 1 will serve as a reference for the interpretation of the results in the following sections. With hourly averages, there are potentially about 124,000 data points per energy channel over the 14 years. However, instrument or telemetry limitations reduce this number. The data coverage is about 68% for the electron channels with the exception of the channel with the highest energy (324 keV), where the data coverage is slightly less than 30%. That is, assuming a similar reduction of the data coverage by 32% as for the lower energy channels due to instrument and telemetry limitations, there are no 324 keV electrons detected for about 38% of the time. The data coverage in the proton channels up to an energy of 1.19 MeV is about 75%. Starting at an energy of 1.39 MeV the data coverage drops monotonically to about 40% at the highest energy of 4.10 MeV. Using the same reasoning as in the case of electrons, there are no protons detected at the highest energies for about 35% of the time. The diminished data coverage at high energies for both electron and proton fluxes indicates that high energetic particles from solar eruptive events are predominantly measured in the channels with the highest energies.

3. Results

3.1. Statistical Studies

This statistical study is based on a 14-year data set of Ulysses HI-SCALE measurements covering the period from 1990 to 2004. In particular, we investigate (1) solar cycle variations of electron and ion fluxes, (2) changes of the energy spectra with the solar cycle, (3) detailed flux distributions as a function of energy, and (4) time-resolved fluxes during periods of intense solar activity.

Monthly average proton and electron fluxes in two energy channels are shown in Figures 2 and 3, respectively, for the 14-year interval. The blue vertical bars in the figures reflect the temporal variations of the flux measurements in each monthly data set and are not measurement errors. The average fluxes are slightly higher in 2001 during the maximum of solar cycle 23 compared to the previous cycle (1991/1992) in contrast to the smoothed monthly sunspot numbers shown in Figure 1. The large variation of the proton fluxes makes it difficult to identify the double peak of the sunspot numbers – a distinct feature of solar cycle 23 – even though some months in 2003 show elevated proton flux values.

Interestingly, the largest monthly variations are found during the solar minimum period from 1995 to 1997. These variations indicate both the spacecraft passage through the heliospheric current sheet during the fast latitude pass (October 1994 – June 1995) as well as contributions from individual solar events, which are superimposed on an otherwise quiet background. The largest monthly variations in the mid-energy (268 keV) electrons typically occur during the solar maximum periods. In addition, the electron fluxes at the solar maxima follow the trend seen in the smoothed monthly sunspot numbers, i.e., the electron flux was higher during the maximum of solar cycle 22.

The flux levels for both protons and electrons differ by about two orders of magnitude between solar minimum and maximum (Figures 2 and 3). On rare occasions this difference might extend to three orders of magnitude. Typical solar minimum fluxes for both the 530 keV protons and the 268 keV electrons are ~ 1 to 2×10^{-3} counts $\text{cm}^{-2} \text{s}^{-1} \text{sr}^{-1} \text{keV}^{-1}$. The corresponding values at solar maximum are about $\sim 2 \times 10^{-1}$ counts $\text{cm}^{-2} \text{s}^{-1} \text{sr}^{-1} \text{keV}^{-1}$.

The proton and electron spectra depicted in Figures 4 and 5 are yearly averages. The flux levels are coded according to the rainbow spectrum, i.e., the highest fluxes are shown in red whereas the lowest fluxes are plotted in violet. The solar maxima and minimum can

easily be identified in the legends to the plot in the upper right corner of the respective figures. As noted in the discussion of Figures 2 and 3, the flux differences between solar maximum and minimum amount to about two orders of magnitude, with somewhat larger spreads in some exceptional cases. This spread is fairly uniform across the entire energy range for both protons and electrons. Note that the 1991 and 2001 proton energy spectra are virtually identical, i.e., the 2001 spectrum is superimposed on the 1991 spectrum. During 1991, Ulysses was in transit in the ecliptic plane between Earth and Jupiter.

The results of a power law fit to the observed yearly energy spectra are given in Table 1. In general, the slope of the energy spectra is not as steep as E^{-2} ; the average exponential coefficients for 15 years (only two months in 1990) are $k = -1.56$ for protons and $k = -1.88$ for electrons, respectively. However, there are some notable exceptions. The steepest proton spectra are encountered in 1992 ($k = -2.14$) and 1999 ($k = -1.87$), which correspond to the declining phase of solar cycle 22 and the ascending phase of the next cycle, respectively. However, the electron spectra show a different behavior. The steepest slopes occur during solar minimum and maximum, when the power law exponent is significantly smaller than -2 . The average 14-year spectral slope for the protons ($k \sim -1.5$) is the slope of the differential energy spectrum that is predicted by Fisk and Gloeckler [2006] if these energy protons are produced by stochastic acceleration due to compressional turbulence in the solar wind. However, a variety of slope values are

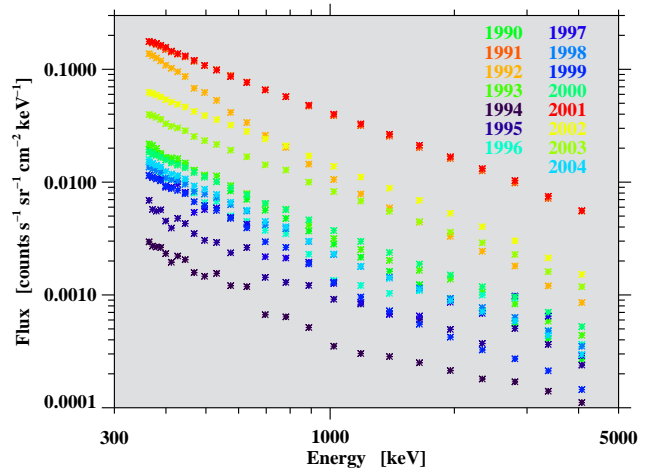


Figure 4. LEFS 150 proton energy spectra from 1990 to 2004.

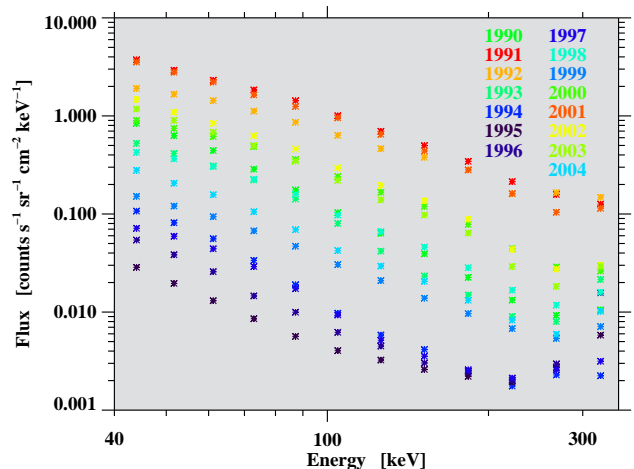


Figure 5. LEFS 150 electron energy spectra from 1990 to 2004.

measured on a yearly average basis, as are tabulated in Table 1. Further, slopes of spectra following individual events can be quite variable in time (not shown here). This interesting topic of the slopes of proton and electron energy spectra in these energy ranges will be discussed in a paper currently in preparation.

Though all power law fits pass a simple χ^2 -statistics test, some caution should be taken in interpreting the results. The largest χ^2 values occur in solar minimum years. A closer inspection of Figures 4 and 5 reveals larger variations at higher energies, indicative of sporadic solar events increasing or modulating the proton and electron fluxes in the high-energy regime.

Analysis of animated time-series of energy spectra with the full temporal resolution (~ 17 min) show a larger variation of the energy spectra, especially, associated with solar events (not shown here). In particular, a single power law fit will no longer produce adequate results for many spectra. Separate fits for the high- and low-energy parts of the spectrum have to be used in such cases. In these instances, the slopes in the low-energy portion of the spectra tend to be steeper. Interestingly, this feature can even be seen in the proton spectrum for 1992 (Figure 4), where several solar events imprint their signature on the entire data set.

Figures 6 and 7 collapse the proton and electron data sets into single plots to provide the frequency of occurrence of flux levels as a function of energy for the entire 14-year interval. Detailed frequency-of-occurrence distributions of proton and electron fluxes are, for example, required in spacecraft and instrument design. In particular, knowledge of such flux distributions are important for missions that will operate for long time periods and encounter a variety of interplanetary conditions. The individual frequency distributions in Figures 6 and 7 are constructed by counting the flux values encountered in equidistantly spaced flux bins on a logarithmic scale (note the equidistant spacing of the surface plot grid lines for the flux axis). At each energy, the frequency distribution is normalized such that the area underneath the curve that includes the measured total flux range is unity; i.e., the figures display relative occurrence frequencies for flux levels at each measured energy. Since the proton energy channels are not equidistantly spaced, neither on a normal nor on a logarithmic scale, the grid lines for the energy axis are more condensed towards low energies. Thus, the energy resolution is higher for low-energy protons. The energy channels for electrons are roughly equidistantly spaced on a logarithmic scale.

Asymmetry is a common feature of both the proton and electron frequency distributions. Since higher energy particles are less prevalent, the frequency distributions are shifted toward lower fluxes at the higher energies. The proton distributions are narrower and more prominently peaked (at low flux counts) at higher energies. In comparison to the electron distributions, the proton curves are fairly smooth and lack any detailed structure. The electron distributions are characterized by three distinct features: (1) a secondary maximum at low fluxes and higher energies, (2) a double-peaked structure at low energies of the main component of the distribution, and (3) a distinct ripple-like feature at large fluxes across the entire energy range.

3.2. Discrete Events

Thus far, only the general statistical properties of low-energy electron and ion fluxes have been described. During solar events much higher fluxes occur and thus have to be considered in the design of spacecraft traveling in the interplanetary medium beyond Earth, to the Moon and on to Mars. In addition, such particles can have an significant impact on the atmosphere and surfaces of Mars and its two satellite moons.

Shown in Figure 8 are high-resolution time profiles of proton fluxes in selected energy channels (364 keV, 1.39 MeV, and 4.10 MeV) during the ‘‘Halloween Events’’ in October/November 2003. The temporal resolution of the spectra is typically either 17 or 34 min. Several X- and M-class flares were observed during this period of intense solar activity. Figure 9 displays time profiles of X-ray fluxes in two energy channels (0.5–4.0 Å and 1.0–8.0 Å) as measured by the GOES 12 spacecraft. Since the three main active

regions NOAA 10484, 10486, and 10488 rotated to the backside of the Sun on 2003 November 5, the X-ray flux sharply declined thereafter. A collection of research papers related to this very prominent example of solar eruptive phenomena and associated space weather effects was assembled in a special volume of *Journal of Geophysical Research* [Gopalswamy *et al.*, 2005].

The large number of flares (10 X-class and more than 30 M-class flares) was one of the remarkable characteristics of the three ‘‘naked-eye’’ sunspot groups in October/November 2003. Many

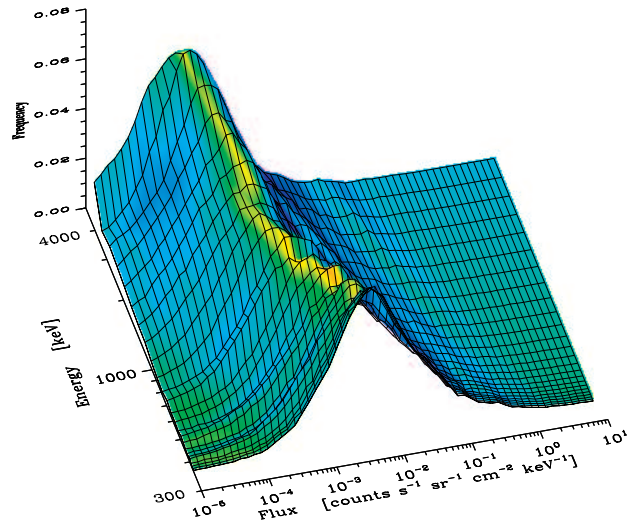


Figure 6. Surface plot of the average LEFS 150 proton flux distributions for individual energy channels during the time period from 1990 to 2004.

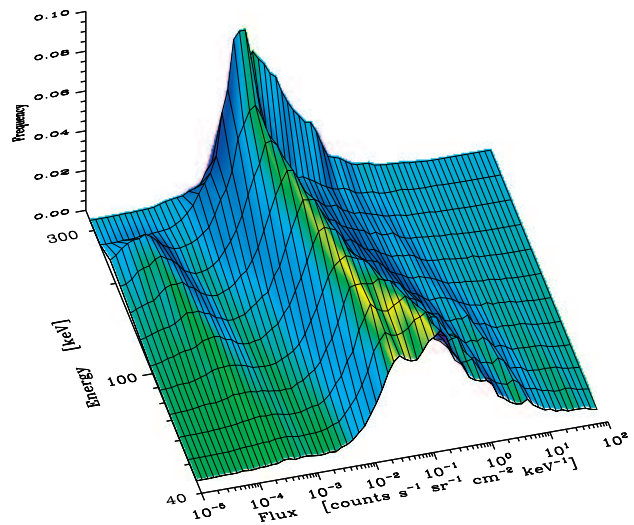


Figure 7. Surface plot of the average LEFS 150 electron flux distributions for individual energy channels during the time period from 1990 to 2004.

CMEs resulted in very intense Solar Energetic Particle (SEP) events, three of which produced Ground Level Enhancements (GLEs). Two of the eruptions were characterized as rare “fast transit” events reaching Earth in less than a day. The increased solar activity from October 25 to 28 led to a gradual rise of the proton fluxes (see Figure 8). Multiple X- and M-class flares produced strong variations in the proton fluxes during that time period. This period of enhanced solar activity also serves as an example of the heliosphere acting as a reservoir for charged particles. The initial activity fills the reservoir within a few days. Thereafter, the particle fluxes remain fairly constant showing only a gradual decrease. Furthermore, only the largest solar events can imprint a distinct signature on the otherwise only slowly varying particle fluxes.

The initial activity phase came to an end when a X17 proton occurred close to disk center at 11:10 UT on October 28, which was followed by a very large and fast halo CME. The proton fluxes increased by more than three orders of magnitude compared to the pre-storm levels on October 25. After this “super storm” the proton fluxes stabilized and slightly declined at levels of about two orders of magnitude higher compared to the pre-storm phase. Interestingly, the low-energy protons (364 keV) started to increase again on November 4, presumably as a result of the X-class flares on November 2 and 3. Before moving off to the backside of the solar disk, NOAA 10486 produced an X28 flare, which led to a renewed increase of the proton fluxes on November 6. The maximum (not shown in Figure 8) was reached between November 10 and 14 approaching values similar to the X17 event on October 28. However, this time the high fluxes continued for several days. The maximum phase was followed by gradual decline until November 23, when the proton fluxes returned to pre-storm levels.

4. Discussion

A prominent example of low-energy protons affecting spacecraft is the detector degradation suffered by the AXAF CCD Imaging Spectrometer (ACIS) on board the Chandra X-ray observatory [Nartallo *et al.*, 2001]. Protons with energies from tens of keV to a few MeV can be scattered by the optics of X-ray telescopes and ultimately reach the focal plane instruments, where they have a negative influence on the Charge Transfer Efficiency (CTE) of CCD detectors. Based on the experience with ACIS, the authors carried out numerical simulations to assess the radiation environment that the Chandra and XMM-Newton X-ray observatories encounter in their highly elliptical orbits during solar maximum conditions. The largest low-energy proton fluxes are typically encountered by these spacecrafts during their transit of Earth’s radiation belts, e.g., 100 keV proton fluxes of about $3 \text{ counts cm}^{-2} \text{ s}^{-1} \text{ sr}^{-1} \text{ keV}^{-1}$ are expected for X-ray telescopes orbiting Earth at 70000 km. These fluxes corresponds to solar wind conditions near solar maximum and/or during periods of intense solar activity for spacecraft leaving the Earth’s protective magnetosphere. Extrapolating the energy spectra shown in Figure 4 to 100 keV yields proton fluxes of about $1 \text{ count cm}^{-2} \text{ s}^{-1} \text{ sr}^{-1} \text{ keV}^{-1}$ for the solar maximum years 1991 and 2001, which have virtually identical energy spectra. Since the slope of the proton spectrum is steeper in 1992 at low energies, the proton flux at 100 keV reaches slightly over $2 \text{ counts cm}^{-2} \text{ s}^{-1} \text{ sr}^{-1} \text{ keV}^{-1}$. Since the interplanetary proton energy spectra measured by Ulysses beyond 1 AU are yearly averages, the instantaneous fluxes at 100 keV will exceed the value of $3 \text{ counts cm}^{-2} \text{ s}^{-1} \text{ sr}^{-1} \text{ keV}^{-1}$ given by Nartallo *et al.* [2001] during solar energetic events.

The non-ionizing energy loss (NIEL) damage to CCD detectors depends primarily on the energy of the protons and thus their penetration depth. The sensitive layer of a front-illuminated CCD is close to the surface of the detector. Therefore, this type of CCD is affected by low-energy (few hundred keV) protons. The sensitive back-illuminated layer resides deeper, and the most damaging protons have energies of $\gtrsim 1.5 \text{ MeV}$. Since photocells and CCD detectors are basically using the same technology, the proton flux data from Figure 4 could be used to assess the potential degradation of

the efficiency of solar panels on spacecraft between Earth and Mars at different phases of the solar cycle.

The effects on surfaces of energetic electrons and protons depend upon the nature of the surface. For insulators, such as semiconductor resists and icy material such as is found on the surfaces of the satellites of the giant planets, electronic sputtering by hundreds of keV to MeV energy protons dominates the modification of such surfaces [e.g., Johnson, 1990]. These energy particles can even determine the lifetimes of icy grains inside the orbit of Jupiter [Lanzerotti *et al.*, 1978] and the lifetime of exposed ice in the polar regions of Earth’s moon [Lanzerotti *et al.*, 1981].

Nuclear collision sputtering is the dominant process for modifying non-insulating materials that comprise the surface materials of spacecraft and non-icy moons and grains. The sputtering cross sections tend to peak at ion energies in the 1 to 100 keV energy range, depending upon the sputtered material and the incident ion species. For example, the sputtering yield for a 10 keV proton on carbon/graphite is $\sim 10^{-2}$. Extrapolating the year 1991/2001 solar maximum proton energy spectra (Figure 4) to $\sim 10 \text{ keV}$ one finds that the proton sputtering rate for a carbon-like surface would be

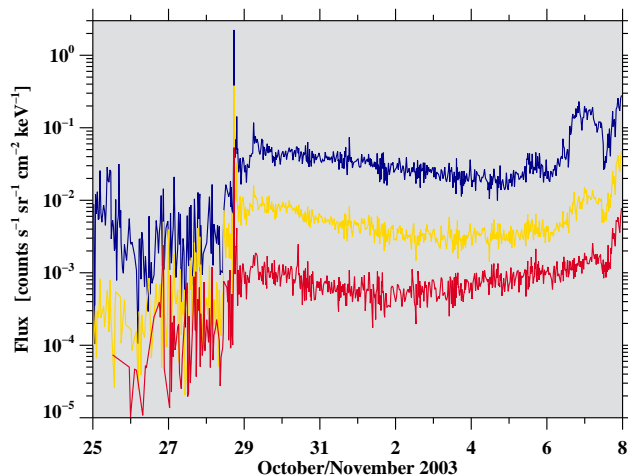


Figure 8. High-resolution time profiles of the proton fluxes during the “Halloween Events” in October/November 2003 obtained in the 364 keV (blue), 1.39 MeV (yellow), and 4.10 MeV (red) energy channels.

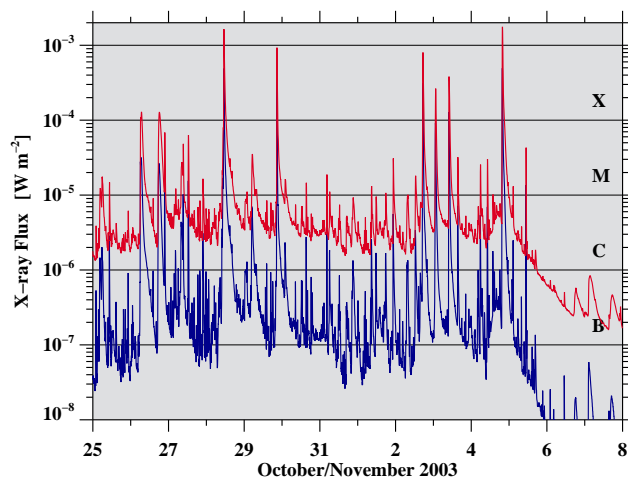


Figure 9. GOES 12 X-ray flux (5-minute data) during the “Halloween Events” in October/November 2003 obtained in the 0.5 – 4.0 Å (blue) and 1.0 – 8.0 Å (red) energy channels.

of the order of $2 \text{ atoms s}^{-1} \text{ cm}^{-2}$, or $\sim 6 \times 10^7 \text{ cm}^{-2}$ over a year. At solar minimum, the sputtering rate would be $\sim 10^{-1} \text{ atoms s}^{-1} \text{ cm}^{-2}$.

In addition to sputtering, energetic ions can cause mixing of regolith materials and changes in adhesion properties [Johnson, 1990]. While damage effects to semiconductors and solar cells by the ions and electrons represented in Figures 4 and 5 can occur over a year or less, and thus affect the operations of instruments and spacecraft, the effects of solar particles on bodies such as the moons of Mars (Phobos and Deimos) will occur over millennia and longer time scales but short on the scale of the age of the solar system.

5. Conclusions

Ulysses is the only spacecraft mission out of the ecliptic and in the heliosphere between Earth's and Jupiter's orbit. Its unique data has contributed enormously to understanding of the heliosphere environment inside 5 AU by investigating solar-produced interplanetary phenomena. This study was motivated by the fact that particle fluxes in energy ranges covered by HI-SCALE can modify spacecraft surface materials as well as the surfaces of natural physical objects in the heliosphere inside Jupiter's orbit, such as grains and the moons of Mars. The results are based on high-resolution interplanetary electron and ion spectra, which were obtained over more than a solar cycle (1990–2004) from $\sim 1.4 \text{ AU}$ to $\sim 5 \text{ AU}$. The signature of the solar cycle is clearly present in the average yearly ion and electron spectra, which both vary by factors of ~ 100 over a solar cycle across the energy ranges measured. The following summarizes the major results of this statistical study of the electron and ion fluxes since the launch of the Ulysses spacecraft:

1. Average yearly ion and electron spectra are not strict power laws, but have some statistically-significant variability across the energy ranges measured.
2. Parameterizing electron and ion energy spectra by power laws shows that yearly average spectra tend to vary less steeply than E^{-2} .
3. Frequency distributions of ion and electron flux values at given energies have spreads of more than two orders of magnitude during a solar maximum year 2001.
4. The statistical results are important for documenting the variability in particle fluxes in the heliosphere beyond Earth's orbit and in the vicinity of Mars.

Acknowledgments. JZR would like to thank the New Jersey Space Grant Consortium for a summer research stipend, which enabled her participation in this research project. We would like to thank Dr. Vasylyshyn for carefully reading the manuscript and valuable comments. This work was supported by NSF under grants ATM 03-42560, ATM 02-36945 and IIS ITR 03-24816, by NASA under grant NAG 5-12782 and by the ACE and Ulysses projects through contracts with the Johns Hopkins University Applied Physics Laboratory.

References

Boufaïda, M. and T. P. Armstrong (1997), Spatial Variations of 0.2 to 5 MeV Protons in the 1–5 AU In-Ecliptic Region From Ulysses, Voyager 1 and 2, and IMP 8 Gradient Studies, *J. Geophys. Res.*, *102*(A4), 7013.

Fisk, L. A. and G. Gloeckler (2006), The Common Spectrum for Accelerated Ions in the Quiet-Time Solar Wind, *Astrophys. J.* *640*, L79.

Foullon, C., N., Crosby, and D. Heynderickx (2005), Toward Interplanetary Space Weather: Strategies for Manned Missions to Mars, *Space Weather*, *3*(7), S07004, doi:10.1029/2004SW000134.

Gold, R. E., S. M. Krimigis, S. E. Hawkins, D. K. Haggerty, D. A. Lohr, E. Fiore, T. P. Armstrong, G. Holland, and L. J. Lanzerotti (1998), Electron, Proton, and Alpha Monitor on the Advanced Composition Explorer Spacecraft, *Space Sci. Rev.*, *86*, 541.

Gopalswamy, N., L. Barbieri, E. W. Cliver, G. Lu, S. P. Plunkett, and R. M. Skoug (2005), Introduction to Violent Sun-Earth Connection Events of October–November 2003, *J. Geophys. Res.*, *110*, A09S00, doi:10.1029/2005JA011268.

Johnson, R. E. (1990), Energetic Charged Particle Interaction with Atmospheres and Surfaces, *Phys. Chem. Space*, *19*, Springer-Verlag, Berlin.

Lanzerotti, L. J., T. P. Armstrong, R. E. Gold, C. G. MacLennan, E. C. Roelof, G. M. Simnett, D. J. Thomson, K. A. Anderson, S. E. Hawkins (1995), Over the Southern Solar Pole – Low-Energy Interplanetary Charged Particles, *Science*, *268*, 1010.

Lanzerotti, L. J., R. E. Gold, K. A. Anderson, T. P. Armstrong, R. P. Lin, S. M. Krimigis, M. Pick, E. C. Roelof, E. T. Sarris, G. M. Simnett, and W. E. Frain (1992), Heliosphere Instrument for Spectra, Composition and Anisotropy at Low Energies, *Astron. Astrophys. Suppl. Ser.*, *92*, 349.

Lanzerotti, L. J., W. L. Brown, R. E. Johnson (1981), Ice in the Polar Regions of the Moon, *Phys. Chem. Space*, *86*, 3949.

Lanzerotti, L. J., W. L. Brown, J. M. Poate, and W. M. Augustyniak (1978), Low Energy Cosmic Ray Erosion of Ice Grains in Interplanetary and Interstellar Media, *Nature*, *272*, 431.

MacLennan, C. G., L. J. Lanzerotti, and R. E. Gold (2003), Low Energy Charged Particles in the High Latitude Heliosphere: Comparing Solar Maximum and Solar Minimum, *Geophys. Res. Lett.*, *30*(19), 8033, doi:10.1029/2003GL017080.

Nartallo, R., E. Daly, H. Evans, P. Nieminen, F. Lei, and P. Truscott (2001), Low-Angle Scattering of Protons on the XMM-Newton Optics and Effects on the On-Board CCD Detectors, *IEEE Trans. Nucl. Sci.*, *48*(6), 1815.

Parker, E. N. (2005), Shielding Space Explorers from Cosmic Rays, *Space Weather*, *3*(8), S08004, doi:10.1029/2005SW000176.

Patterson, J. D. and T. P. Armstrong (2003), Steady-State Event-Excluded Proton Spectra at Solar Minimum at All Heliolatitudes, *Geophys. Res. Lett.*, *30*(19), 8037.

Patterson, J. D. (2002), An Analysis of Solar Energetic Particle Spectra Throughout the Inner Heliosphere, *Ph. D. Thesis*, University of Kansas, Lawrence, Kansas.

Roelof, E. C., R. E. Gold, G. M. Simnett, S. J. Tappin, T. P. Armstrong, and L. J. Lanzerotti (1992), Low-Energy Electrons and Ions Observed at Ulysses February–April, 1991: The Inner Heliosphere as a Particle Reservoir, *Geophys. Res. Lett.*, *19*(12), 1243.

Simpson, J. A., and 19 co-authors (1995), Cosmic Ray and Solar Particle Investigations Over the South Polar Regions of the Sun, *Science*, *268*, 1019.

Simunac, K. D. C. and T. P. Armstrong (2004), Solar Cycle Variations in the Solar and Interplanetary Ions Observed with Interplanetary Monitoring Platform 8, *J. Geophys. Res.*, *109*, A10101, doi:10.1029/2003JA0101194.

C. Denker, New Jersey Institute of Technology, Center for Solar-Terrestrial Research, 323 Martin Luther King Blvd, Newark, NJ 07102, USA. (cdenker@adm.njit.edu)

J. Z. Reza, New Jersey Institute of Technology, Center for Solar-Terrestrial Research, 323 Martin Luther King Blvd, Newark, NJ 07102, USA. (jzr2@njit.edu)

A. J. Nelson, New Jersey Institute of Technology, Center for Solar-Terrestrial Research, 323 Martin Luther King Blvd, Newark, NJ 07102, USA. (ajn9@njit.edu)

J. D. Patterson, Fundamental Technologies, 2411 Ponderosa, Suite A, Lawrence, KS 66046, USA. (patterson@ulysses.ftecs.com)

T. P. Armstrong, Fundamental Technologies 2411 Ponderosa, Suite A, Lawrence, KS 66046, USA. (armstrong@ftecs.com)

C. G. MacLennan, Bell Laboratories, Lucent Technologies, 600 Mountain Avenue, Murray Hill, NJ 07974, USA. (cgm@lucent.com)

L. J. Lanzerotti, New Jersey Institute of Technology, Center for Solar-Terrestrial Research, 323 Martin Luther King Blvd, Newark, NJ 07102, USA. (louis.j.lanzerotti@njit.edu, ljl@lucent.com)